JACS
JOURNAL OF THE AMERICAN CHEMICAL SOCIETY

Article

pubs.acs.org/JACS

DNA-Mediated Morphological Control of Pd−Au Bimetallic Nanoparticles

Nitya Sai Reddy Satyavolu, Li Huey Tan, and Yi Lu*

Department of Chemistry, University of Illinois at Urbana—Champaign, Urbana, Illinois 61801, United States

Supporting Information

ABSTRACT: Recent reports have shown that different DNA sequences can mediate the control of shapes and surface properties of nanoparticles. However, all previous studies have involved only monometallic particles, most of which were gold nanoparticles. Controlling the shape of bimetallic nanoparticles is more challenging, and there is little research into the use of DNA-based ligands for their morphological control. We report the DNA-templated synthesis of Pd−Au bimetallic nanoparticles starting from palladium nanocube seeds. The presence of different homo-oligomer DNA sequences containing 10 deoxy-ribonucleotides of thymine, adenine, cytosine, or guanine results in the growth of four distinct morphologies. Through detailed kinetic studies by absorption spectroscopy, scanning electron microscopy (SEM) and scanning transmission electron microscopy (STEM), we have determined the role of DNA in controlling Pd−Au nanoparticle growth morphologies. One major function of DNA is affecting various properties of the incoming metal atoms, including their diffusion and deposition on the Pd nanocube seed. Interestingly, nanoparticle growth in the presence of A10 follows an aggregative growth mechanism that is unique when compared to the other base oligomers. These findings demonstrate that DNA can allow for programmable control of bimetallic nanoparticle morphologies, resulting in more complex hybrid materials with different plasmonic properties. The capability to finely tune multimetallic nanoparticle morphology stems from the versatile structure that is unique to DNA in comparison to conventionally used capping agents in colloidal nanomaterial synthesis.

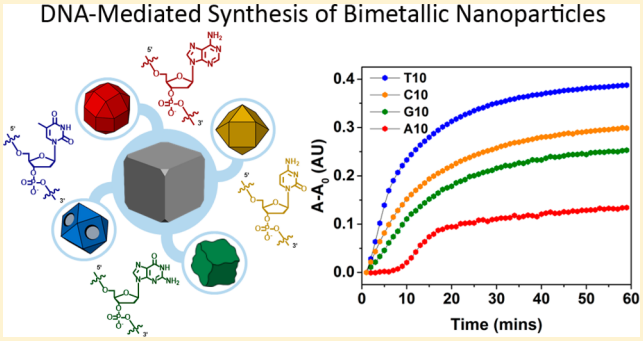

INTRODUCTION

Colloidal metal nanoparticles have been widely employed in many applications including catalysis,[1] sensing,[2] photonics,[3] and medicine.[4] Major factors in determining the efficacy of these materials for their applications are the different shapes and surface properties these nanoparticles exhibit. Therefore, being able to control the morphology of metal nanoparticles is critical for their successful application. An effective strategy to control nanoparticle morphology is to use different capping ligands during the synthesis of the nanoparticles.[5] In addition to providing colloidal stability, the ligands, depending on their binding affinity to the seed or precursor used, can often influence the rates of precursor reduction and diffusion as well as facet stabilization and can also in some conditions serve as reducing agents themselves.[5]

Among the known biomolecular capping ligands,[6] nucleic acids have a unique programmable ability through different combinations of nucleotide sequences that has been exploited extensively in the field of nanotechnology.[7] Due to the ease of synthesis of this biopolymer, it can be modified easily and thus be coupled to many nanomaterial systems.[7e,f,8] Therefore, we and others have demonstrated that DNA can be used to control the shape, and thus the properties, in a sequence-dependent manner of monometallic systems such as gold[9] and silver[10] nanoparticles. However, all previous studies using DNA as the ligand have involved only monometallic particles. Bimetallic nanoparticles have attracted interest not only due to their multifunctionality but also because of their synergistic properties.[11] Furthermore, while extensive studies have been performed on the interaction of DNA with Au surfaces,[12] similar studies with other metals are rare. Understanding the growth mechanisms of bimetallic systems in the presence of DNA can give us important information about whether DNA synergistically or independently interacts with the two metals.

Pd−Au bimetallic nanoparticles are particularly interesting due to their catalytic properties for a variety of reactions, such as vinyl acetate synthesis[13] and oxidation of alcohols to aldehydes.[14] The lattice mismatch between Au and Pd is reasonably low (~4.9%), and their ability to be coreduced in an identical reducing environment despite difference in redox potentials ($AuCl_4^-$ /Au: 1.002 V and $PdCl_4^{2-}$/Pd: 0.591 V)[15] makes them an ideal system to study. In the synthesis of Au−Pd bimetallic nanocrystals, the roles of various factors such as anions, pH,[16] and shape of the seed[17] have been studied comprehensively. While all these factors greatly influence the

Received: October 20, 2016
Published: November 22, 2016

DOI: 10.1021/jacs.6b10983
J. Am. Chem. Soc. 2016, 138, 16542−16548

shape of the nanocrystal, not many studies have focused on the effect of different capping agents for the synthesis of these particles of controlled architecture. Ligands that are conventionally employed in the synthesis of metallic nanomaterials are largely limited in the variability of their functional groups. DNA, on the other hand, can have a great deal of functional variance due to its high sequence variability and the structural complexity associated with it.

In this study, we extend the application and demonstrate the effect of DNA as a capping ligand to control the morphologies of bimetallic structures starting with palladium nanocubes as seeds, resulting in four unique morphologies that were governed by the specific homo-oligonucleotide sequence used. We further studied the interaction of DNA with Pd, an area that has not been investigated thoroughly. Through detailed characterization and kinetic studies, we were able to decipher how different DNA sequences control the morphologies of bimetallic nanoparticles through modulation of DNA affinities for, and diffusion on, the metal surfaces. Additionally, we have also demonstrated that the difference in affinities is highly influential in determining the mechanism of metal deposition onto the core.

RESULTS AND DISCUSSION

DNA Sequence Dependent Morphology Control of Palladium–Gold (Pd–Au) Nanoparticles. In order to investigate the potential roles of DNA sequences in controlling the morphologies of bimetallic nanoparticles, we first synthesized palladium nanocubes (~65 nm, Figure S1) using a slightly modified protocol (see Experimental Section) from that reported previously[18] and then employed them as seeds to synthesize Pd–Au nanoparticles in the presence of different DNA molecules. Seed-mediated synthetic routes to form core–shell bimetallic nanostructures have proven to be a straightforward method to obtain monodisperse samples.[19] Coreduction of gold and palladium precursors ($HAuCl_4/H_2PdCl_4$ = 10:1) at room temperature using a mild reducing agent, hydroxylamine (NH_2OH), was performed in the presence of homo-oligomers containing 10 deoxy-ribonucleotides of thymine, adenine, cytosine, or guanine (referred to as T10, A10, C10, and G10, respectively, hereafter). The use of homo-oligomeric sequences helps us decouple parameters, such as base-dependent binding affinity, from others. In previous studies,[9b] we have determined that 10 is the minimal length to keep nanoparticles colloidally stable while controlling the morphologies of the nanoparticles. Therefore, we chose A10, T10, C10, and G10 for this study. In comparison to previous studies in which 30 bases of DNA molecules were used, a higher concentration of DNA was used (see Experimental Section), in order to compensate for the shorter length of DNA (10 bases) adopted in this study, and to ensure sufficient interactions between DNA and all the components (seed and precursors) of the system. The reaction was subsequently allowed to proceed for 24 h. As shown in Figure 1, coreduction in the presence of T10 resulted in formation of a cuboctahedron core-frame, with the {100} surface of the cubic core exposed—a unique morphology that has not been observed before for Pd–Au bimetallic nanostructures to our knowledge. On the other hand, the presence of A10 promoted the formation of rhombicuboctahedron particles, C10 allowed the formation of cuboctahedron particles and G10 permitted the formation of nanoparticles where the Pd–Au shell covers the Pd core surface in an uneven manner (Figure 1). In the absence of any DNA molecule, aggregated particles of Pd and Au were observed (Figure S2), confirming the role of DNA in both influencing the final morphology and maintaining colloidal stability of the particles.

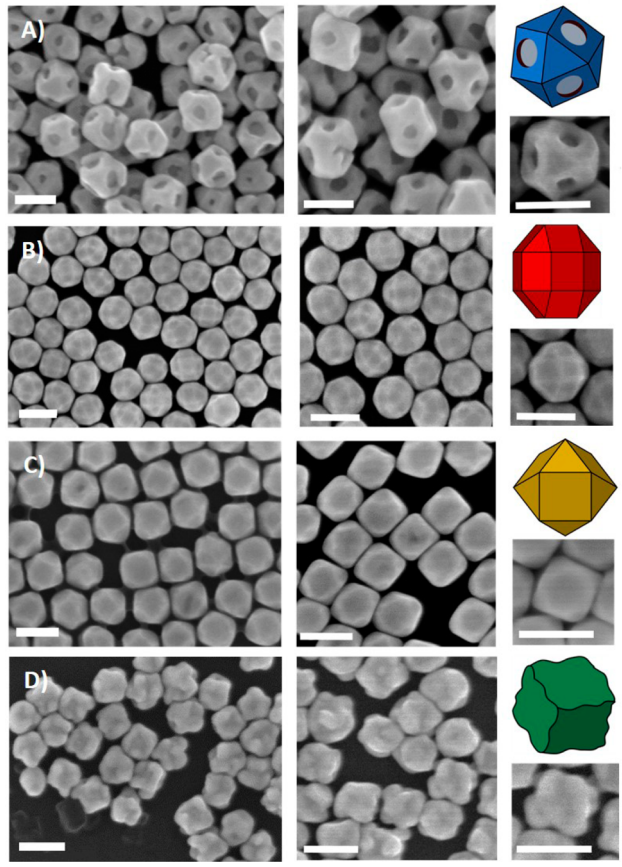

Figure 1. SEM images of the Pd–Au nanoparticles synthesized in the presence of (A) T10, (B) A10, (C) C10, and (D) G10. Scale bars = 100 nm.

To study the elemental compositions of the core and shell for each morphology obtained, we used STEM-EDS (Energy dispersive spectroscopy) analysis (Figure 2). The elemental

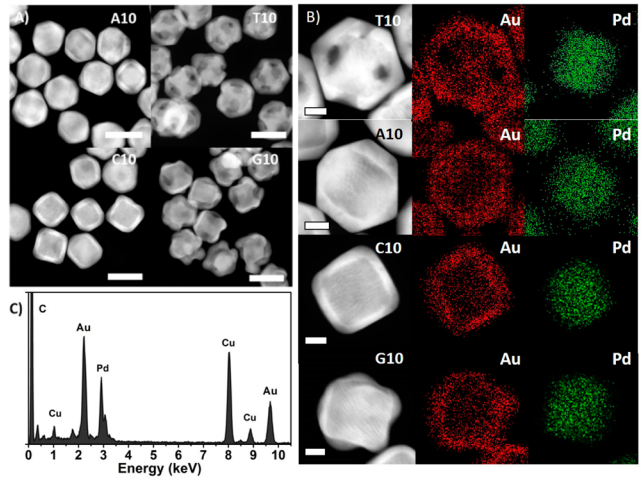

Figure 2. (A) STEM images of each of the particles. Scale bars = 100 nm. (B) Elemental map for each morphology, indicating the composition of the final particles. Scale bars = 25 nm. (C) EDS of a G10 particle.

DOI: 10.1021/jacs.6b10983
J. Am. Chem. Soc. 2016, 138, 16542–16548

map reveals that the Pd nanocube clearly resides at the center of each structure, while the shell contains both Pd and Au, with Au in excess. Since the precursors were used in a ratio of 10:1 ($HAuCl_4/H_2PdCl_4$) in the coreduction process, this observation of excess Au in the shell was expected. Additionally, when only $HAuCl_4$ was used as the precursor (with A10 and T10 sequences), the Au was confined to the shell and Pd to the core (Figure S3). The data indicate that the Pd precursor plays no significant role in influencing the morphology, but it does influence the composition of the shell (see Figures 2b and S4). The powder X-ray diffraction (PXRD) analysis of the particles (Figure S4) showed a shift in the pure Au peaks, indicating the presence of a small amount of Pd in the mostly Au shell.

The most interesting shape was obtained in the presence of T10, wherein a Au−Pd core-frame was formed over the Pd cubic seed. The SEM, STEM, and EDS elemental maps clearly show the retention of the cubic core with the {100} facet exposed, suggesting that the addition of reducing agent favors the direct reduction of Au and Pd precursors. STEM and EDS elemental map data representing different angles of the core-frame structure have also been collected (Figure S5). The rhombicuboctahedron particles formed in the presence of A10 display three surfaces, as confirmed by Selected Area Electron Diffraction (SAED, Figure S6) and as observed by SEM, namely {100}, {111}, and the {110} facets. In contrast, the cuboctahedron nanoparticles fomed in the presence of C10 consist of only two distinct facets: the {100} and the {111} facets (Figure S7). The G10 mediated particles exhibit an unusual shape owing to the undulated Pd−Au shell over the cubic core.

All the particles were obtained in high yield and exhibited plasmonic properties in the visible region with λ_{max} values between 500 to 600 nm. The T10-mediated particles displayed the most red-shifted peak at around 595 nm while the A10 mediated particles had the most blue-shifted peak at around 528 nm. The spectra of C10 and G10 mediated particles were very similar to each other, with λ_{max} consistently between those of A10 and T10 mediated particles (Figure S8).

Kinetics of DNA Mediated Nanoparticle Growth. To elucidate the roles of each DNA sequence in forming these unique shapes, the kinetics of the nanoparticle formation were monitored by absorption spectroscopy in the visible region. Seeded growth can be monitored by the absorbance of the surface plasmon peak, which is directly related to the volume fraction of the nanoparticles grown as a function of time.[20] Since it is known that Pd exhibits a very weak localized surface plasmon resonance (LSPR) as compared to metals such as Au or Ag, the majority of the contribution to the obtained SPR is from Au. Additionally, since the emergence of the LSPR of the shell with time remained consistent through the growth, it helped us monitor the change of absorbance and thus the deposition of gold in a consistent manner. The final LSPR peak positions and the full width at half maximum (fwhm) of each of the spectral profiles obtained were different owing to the differently shaped bimetallic particles. The Pd core itself exhibited a weak plasmonic peak around 400 nm initially (Figure S9), and with time, a new plasmonic peak between 500 and 600 nm appeared (Figure S10). The increase in absorbance of the spectra depended on the sequence used for the growth. This sequence-dependent rate increase became more evident when the λ_{max} values for each sample were plotted against time (Figure 3B).

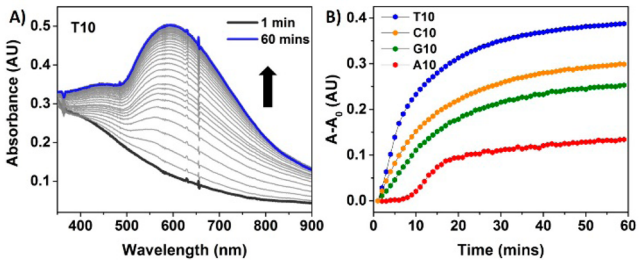

Figure 3. (A) Kinetic UV−vis absorption spectra of nanoparticle growth in the presence of T10. (B) The plot of absorbance vs time at the λ_{max} values for each of the particles.

Figure 3B shows that, while the kinetic profiles of nanoparticle growth under the influence of T10, C10, and G10 are very similar, the rates of increase are different, with the T10 particles having the highest rate and the G10 particles having the lowest rate. It should be noted that the absorbance of the particles is sensitive to the morphology. The extinction coefficient may change as the particles grow in solution, and that may contribute to a possible deviation. However, the trend of absorbance increase for T10, C10, and G10 remains the same. In contrast, the A10 mediated particles show a unique sigmoidal growth profile for the initial time points (0−25 min), which is distinct from those of the above three particles, in addition to having a lower rate of absorbance increase (Figure 3B). To corroborate our analysis, the area under each spectrum (between 400 to 900 nm) for each time point that we have collected for the growth in the presence of each homo oligomeric sequence was integrated. The trend that we obtained for the integrated areas is the same as that obtained using the LSPR peak height (Figure S11). The kinetic curves were fit using the KJMA (Kolmogorov−Johnson−Mehl−Avrami) model (Figure S12), which has widely been adopted to describe the kinetics of crystallization of materials.[20,21] From this fit, kinetic parameters for the growth in the presence of all the bases were obtained (Supporting Information: Additional information on the UV−vis kinetic studies, Table S1).

A sigmoidal growth profile may be indicative of an aggregative growth mechanism.[22] In such a growth mechanism, instead of direct reduction of the precursor onto the seed, there is a nucleation step in which formation of smaller nanocrystallites occurs, after which a preferential interparticle aggregative coalescence takes place. The smaller particles subsequently crystallize onto larger particles, a process known as Ostwald ripening.[21b] It is known that adenine has a high binding affinity to the gold precursor,[23] and this property of A10 may facilitate the formation of smaller nanoparticles before they aggregate and deposit onto the palladium seed. Such a growth mechanism has been observed for gold nanoparticles stabilized by ligands with strong affinity for Au, such as thiols.[22a] This mechanism was further confirmed when the sample growth was analyzed with HR-TEM after the reduction was quenched at 5 min. The presence of smaller nanocrystallites was clearly observed in the sample (Figure S13). The analysis was carried out only after having washed the sample a minimum of three times. Hence, the possibility of production of smaller nanocrystallites due to the reduction of the Au/Pd precursor by the electron beam unlikely.

In order to monitor the shape evolution during the kinetic growth observed by the above UV−vis spectral changes, we quenched the reduction at different time points with excess 3-

DOI: 10.1021/jacs.6b10983
J. Am. Chem. Soc. 2016, 138, 16542−16548

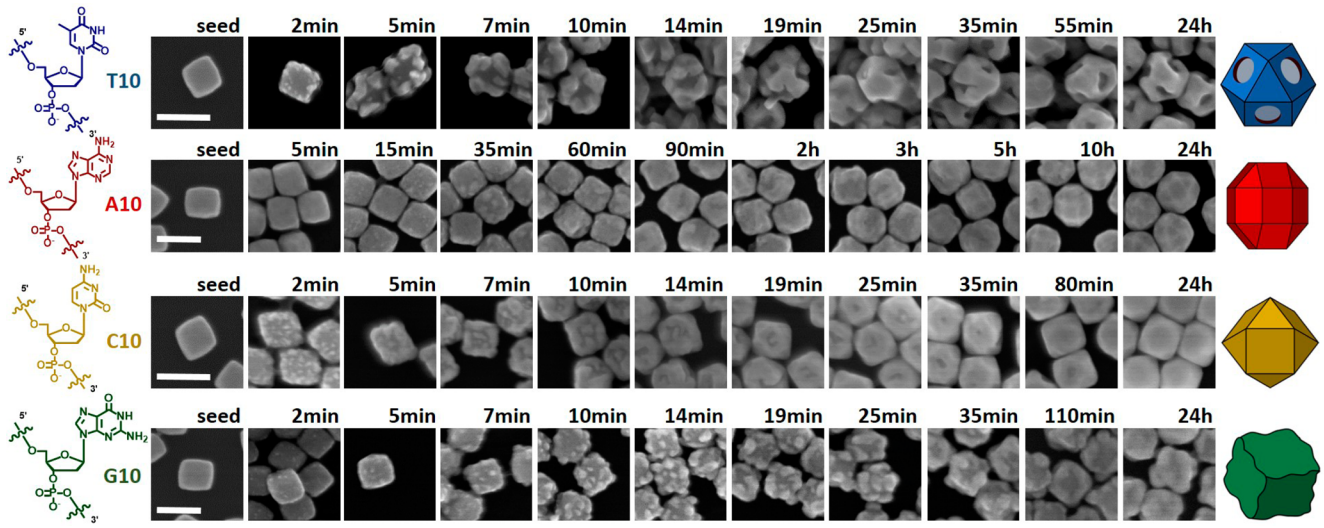

Figure 4. SEM images of the nanoparticle growth quenched at different time points. Time points were chosen to represent the morphology evolution in the presence of each of the poly bases. Scale bars = 100 nm.

Scheme 1. Proposed Mechanism of Growth of Pd–Au Bimetallic Nanostructures Influenced by Different Sequences of DNA[a]

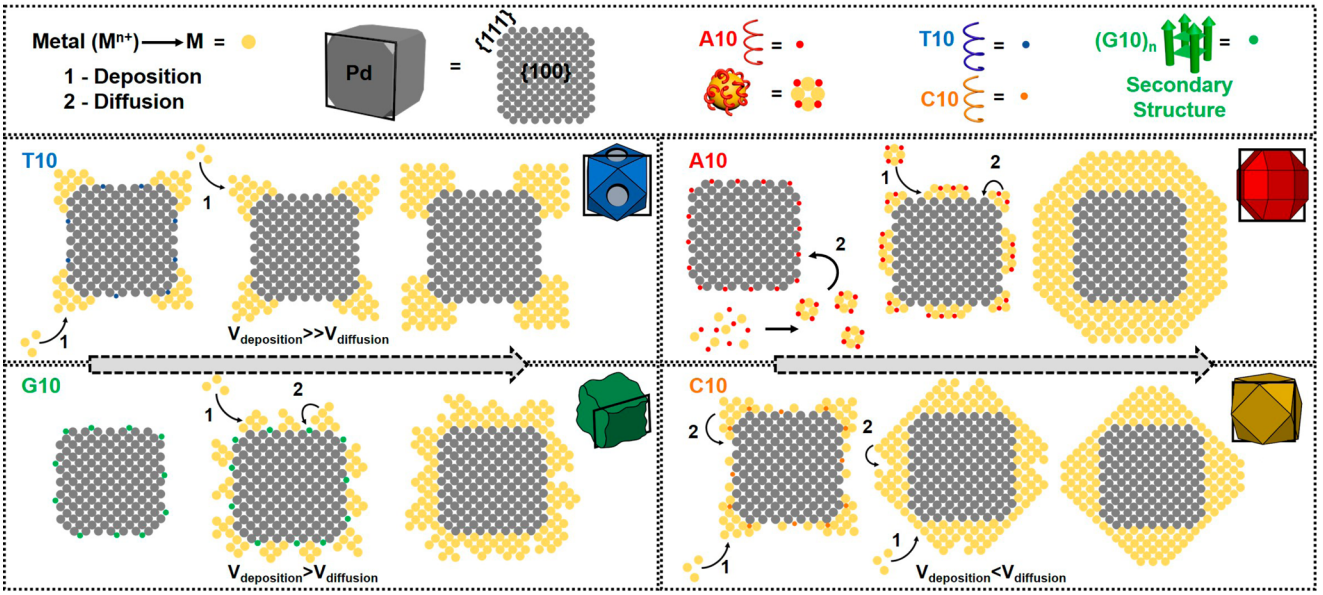

[a]The atomic models represent the cross-section of the 3-D models along the black box in each individual case.

mercaptopropionic acid (MPA), which can bind to the unreacted precursor and prevent further deposition of the metal. Additionally, the reaction mixture after MPA addition was immediately centrifuged to remove any "free" precursor and prevent any further reduction events. SEM was then used to characterize the particle growth quenched at different time points (Figure 4). In all cases, the reaction proceeds via an island-like nucleation of metal on the Pd cube which eventually becomes an epitaxial shell. Based on the above SEM study of the kinetics of the bimetallic particle growth, we propose a scheme (Scheme 1) that illustrates the DNA-mediated mechanism based on the atomic model previously described by Xia and co-workers.[11d,24] The island-like growth may be attributed to a combination of several factors,[11d] including lattice strain, kinetic parameters such as low reaction temperature, and the nature of the seed's surface (e.g., adsorbed ligands[25] such as DNA in this study). In the case of T10 particles, the growth occurs only at the edges and the vertices of the cubic seed, namely the {110} and {111} sites, which eventually transitions to an epitaxial layer in ~20 min. Typically, the deposition of atoms takes place in regions of higher surface free energy (γ), and in this case, the {111} and {110} sites or the vertices and edges of the cube, owing to the lower coordination number of the residing atoms. Thymine can effectively interact with the seed and the precursors through the carbonyl groups.[26] The interaction of the ring-based nitrogen is limited by the electronic effects induced by the adjacent carbonyl groups. The weak interaction between the metal seed and the T10 sequence allows the deposition of metal atoms onto the high-energy sites. Since the deposition rate of atoms is greater than that of the diffusion of atoms to the {100} facet, which has lower surface free energy, the formation of the satellite core-frame bimetallic nanostructure takes place (Scheme 1). In contrast, growth in the presence of the other

DOI: 10.1021/jacs.6b10983
J. Am. Chem. Soc. 2016, 138, 16542–16548

three base oligomers shows nucleation on all the facets of the cube, including the {100} facets. It is known that the passivation of a specific facet by the chemisorption of a capping agent may decrease the surface free energy of that facet. The binding affinity and coverage density of the ligand on the seed determine the extent of lowering the surface free energy. Therefore, the affinity of the DNA bases to the higher energy sites and the subsequent lowering of γ plays an important role in the formation of the obtained structures, making the growth a kinetically controlled process.

Growth in the absence of DNA also provides important evidence for the above hypothesis. The particles formed in the absence of DNA contain Pd−Au structures that have the Pd {100} facet exposed, even though the particles aggregated (Figure S2). The formation of such a shape indicates that the incoming metal preferentially covers the edges and the corners of the cubic seed, i.e. the sites that have high energy as compared to the {100} faces of the cube. In the presence of a capping agent, there may be lowering of γ that results in a variable deposition profile.

Our observations for growth in the presence of A10 confirm an aggregative growth route (Scheme 1). Formation of smaller nanocrystallites was not observed in our previous report, where the reduction of gold precursor on gold seeds was studied.[9b] In the previous report, where Au spherical seeds were used, the concentration of A30 DNA was 1 μM and the maximum theoretical number of DNA strands per spherical Au seed was ∼4000 strands. In the current study the amount of A10 DNA used is 12.5 μM, and the number of A10 molecules present per Pd seed is $\sim 6 \times 10^6$ (see calculation in Supporting Information). With a low number of DNA molecules per seed in the previous report, the reduction of gold precursor on gold surfaces is catalytically enhanced.[27] In contrast, the higher number of A10 DNA per seed in the current study can hinder accessibility of metal atoms to directly deposit onto the seed. As a result, the activation energy of direct Au reduction and deposition onto the seed is higher than the activation energy required for the self-nucleation of gold precursors into nanocrystalites. Owing to the exocyclic amine group and the ring-based nitrogen in adenine's structure, A10 tends to have a higher binding affinity to both the precursors and the seed.[26] The passivation of the high-energy sites by A10 is relatively stronger as compared to the other base oligomers. Hence, the deposition and diffusion of atoms on the palladium seed is more uniform on all three facets, ({111}, {110}, and {100}), contrary to the growth modes of the other bases. The direction of growth of the shell is, therefore, along the ⟨111⟩, ⟨110⟩, and ⟨100⟩ directions, which results in the formation of a rhombicuboctahedron, characterized by the {111}, {110}, and {100} facets.

The formation of the cuboctahedron in the presence of C10, as mentioned earlier, proceeds in an early time point (2 min), via nucleation on all facets of the cube. Both guanine and cytosine bases can bind to metal atoms via the carbonyl groups and the exocyclic amine groups.[26] As the growth proceeds in the presence of C10 the deposition of atoms along the {111} and {110} sites is faster than the deposition and diffusion to the {100} facets (Scheme 1). This deposition profile indicates the binding affinity of C10 to the seed is higher when compared to T10. The particles, thus exhibited a crater-like feature in the deposited shell until about 35 min of growth at the center of the {100} facet. Eventually, formation of the fully covered particle takes place. The nanoparticle growth in the presence of G10 to form an undulated shell covering the cubic core is quite peculiar. A detailed inspection of the shape evolution in Figure 4 revealed that, although nucleation occurs on all of the facets, the deposition of the incoming metal occurs only on the already nucleated sites, leading to formation of an undulated shell. The relatively slow kinetics of particle growth in the presence of G10 as compared to that of T10 or C10 may be attributed to the favorable interaction of G10 to the palladium or gold precursors. It is also known that the guanosine base can bind to Pd(II).[28] Additionally, formation of secondary structures such as G-quadruplexes cannot be ignored, and we do observe such a formation in our system (Figure S14). Passivation of the surface by these secondary structures allows deposition of metal on the surface of the seed only in areas that are nonpassivated (Scheme 1). Deposition in secluded areas on the seed subsequently enables the formation of clumpy islands as observed at time points 10, 14, and 19 min in Figure 4. While surface passivation does presumably limit atom diffusion to other areas on the seed, it does not completely eliminate it. Hence, the formation of a shell that is undulated, but that covers the Pd cubic core, takes place. A further increase in the concentration of G10 shows complete passivation of the surface of the cube where there is hardly any deposition of metal onto the Pd core observed (Figure S15).

CONCLUSION

In this study, we have investigated the DNA-mediated morphology control of Pd−Au bimetallic nanostructures and found that the differences in binding affinity of the DNA bases employed determines the extent of passivation of higher energy facets on the palladium nanocube seed. An important factor in the growth is the facets displayed by the seed. The coordination number of the atoms determines the surface energies of the facets. The differential binding of DNA to each of these facets determines the extent of lowering of surface energy. The DNA sequence is also involved in controlling diffusion of the metal atoms in the solution as well as onto the seed. These effects have led to the formation of four unique morphologies of bimetallic Pd−Au nanostructures. Exclusively, A10 initiates an aggregative growth mechanism due to its high binding affinity to the gold precursor. While it is well-known that polyadenine has the highest binding affinity to gold precursors/surfaces,[12] we were able to demonstrate that a reasonably short sequence such as A10 can trigger the formation of smaller individual crystallites before they deposit onto the seed.

In conclusion, the interaction of DNA molecules with the two metals is a dynamic process that depends heavily on the sequence of DNA and the identity of the metal. This dynamic process involves independent interactions of the specific DNA sequence with the Pd present in both the precursor and the seed and the Au present only in the precursor. This conclusion is supported by two main findings in this study: (1) The binding of the DNA to the Pd seed lowers the surface energy in a sequence dependent manner and thus allows differential deposition profiles of Au and Pd on the seed. The lowering of surface energy occurs due to binding events which correlate to the binding affinity of the specific DNA sequence to the Pd seed. Specifically, A10 lowers the surface energy the most, forming a rhombicuboctahedron, while T10 lowers the surface energy the least, resulting in the formation of a core-frame structure. (2) The interaction of DNA molecules with the metal precursors also plays a significant role, allowing A10 to form smaller nanocrystallites before they deposit onto the seed and

DOI: 10.1021/jacs.6b10983
J. Am. Chem. Soc. 2016, 138, 16542−16548

G10 to form secondary structures that passivate the seed surface ultimately forming an undulated core−shell structure.

The system studied herein provides a fundamental understanding of how different DNA sequences influence the final morphology of a system consisting of two disparate metals. The findings of this study can be applied to synthesize more complex hybrid materials using DNA as a capping agent. The ability to control the nanoparticle morphology with such precision can prove to be highly advantageous for many complex systems that can be exploited for energy-related, biomedical, or optical applications.

EXPERIMENTAL SECTION

Materials. All of the chemical reagents were used without further purification. Palladium(II) chloride ($PdCl_2$, 60% Pd basis), hydrogen tetrachloroaurate (III) hydrate ($HAuCl_4{\cdot}xH_20$, 99.9%), cetyltrimethylammonium bromide (CTAB, ≥ 99%), L-ascorbic acid (≥99%), sodium iodide (NaI, 99.5%), hydrochloric acid (HCl, 37%), sodium hydroxide (NaOH, 99.99% trace metal basis), and hydroxylamine hydrochloride ($NH_2OH{\cdot}HCl$, 99.999% trace metal basis) were purchased from Sigma-Aldrich. Deionized water (18.2 MΩ) was used in all procedures. All oligonucleotides used in this study were purchased from Integrated DNA Technologies (Coralville, IA).

Synthesis of 30 nm Cubic Pd NC Substrates. Pd NCs were synthesized by following a previously reported protocol.[18b] Diluted HCl is added to $PdCl_2$ (in 2:1 ratio) to produce a 10 mM H_2PdCL_4 solution. Briefly, a vial containing CTAB (0.05 g) and 9.300 mL of deionized water was sonicated until the CTAB was completely dissolved. Pd precursor (0.500 mL of 0.01 M H_2PdCl_4) was added to the solution, and a bright orange color was produced indicating the formation of the precursor complex with CTAB. The solution was then mixed, and 0.200 mL of 0.1 M NaI was added to the solution. A color change from bright-orange to a dark-red color was observed after iodide addition. The solution was then heated for 5 min at 95 °C with gentle stirring (∼200 rpm), after which 0.200 mL of 0.04 M ascorbic acid was added to the vial. The solution was left to heat for an additional 30 min at 95 °C with stirring until the dark red color was completely replaced by a dark-brown color, which indicated the completed formation of the NC substrates. The solution was removed from heat and stored at 30 °C.

Synthesis of ∼65 nm Cubic Pd NC Substrates. Pd NCs were synthesized by following a previously reported protocol with modifications.[18a] Briefly, CTAB (91.12 mg) was dissolved in 5 mL of Millipore water and transferred to a 15 mL tube. This solution was placed in a water bath at 50 °C for 5 min. To this solution, a Pd precursor (0.125 mL of 0.01 M H_2PdCl_4) was added and mixed well. The previously prepared 30 nm Pd cube seed solution (70 μL) was then added to the above solution and mixed well. Finally, ascorbic acid (25 μL, 0.1 M) was then added to the solution and the reaction contents were mixed vigorously and then kept at 50 °C. The reaction was left to remain still for 14 h until the reaction was complete. These particles were then used for the DNA-mediated synthesis.

DNA-Mediated Synthesis of Pd−Au Bimetallic Nanocrystals. Typically, the ∼65 nm cube solution was first washed by centrifugation (8 krpm for 5 min) to remove the existing CTAB as much as possible. The washed solution was then diluted to have an absorbance of 0.3 at around 400 nm (concentration ∼4.6 ppm Pd as determined by ICP-MS). Then, 85 μL of the diluted solution were incubated in oligomeric sequences of DNA for around 15 min (A10, T10, G10, and C10). The final concentrations of DNA are 17 μM for T10, G10, and C10 and 12.5 μM for A10). Millipore water was added such that the final volume of the entire reaction mixture (including reductant and precursor) is 100 μL. A 200 mM $NH_2OH{\cdot}HCl$ solution was adjusted to pH 5 by using a conc. solution of NaOH. 0.6 μL of this pH adjusted solution was then added to the DNA incubated cubes and then 4 μL of a mixture containing 5 mM $HAuCl_4$ and 0.5 mM H_2PdCl_4, and the reaction is left to completion.

Kinetic Study. In order to arrest the growth of a sample at a certain time point, 1 μL of 3-mercaptopropanoic acid (100 mM, MPA) was added to the solution along with 10 μL of 0.2% SDS. The sample was then subjected to centrifugation and washed with Millipore water 3 times before characterizing using SEM or TEM.

Instrumentation and Characterization. Samples were washed several times (at least three times) with DI water before preparing samples for SEM, TEM, and energy-dispersive X-ray spectroscopy (EDX) spectroscopy. For TEM, 4.0 μL of diluted particle solution were drop-casted onto carbon-coated copper grids, which were then allowed to dry open to the air. The instruments used for TEM and EDX were JEOL 2100 TEM and JEOL 2010F EF-FEG accompanied by an EDX attachment, both operated at 200 kV. Samples for SEM were prepared by placing a 2.5 μL droplet on a silicon wafer and allowing it to dry. SEM was performed using a Hitachi S4800 SEM. A Bruker D8 Venture (DUO) diffractometer was used to obtain the powder XRD patterns. Samples for XRD were prepared lyophilizing concentrated solutions of nanoparticles. The UV−Vis spectroscopy was performed on an HP 8453 UV−vis spectrophotometer. Images were edited using ImageJ software. Circular dichroism (CD) experiments were carried out with a Jasco J-810 spectropolarimeter equipped with a Julabo temperature controller. PerkinElmer - SCIEX ELAN DRCe ICP-MS was used to perform ICP-MS on the seed solutions.

ASSOCIATED CONTENT

Supporting Information

The Supporting Information is available free of charge on the ACS Publications website at DOI: 10.1021/jacs.6b10983.

Additional notes on fitting of kinetic data, characterization of seed and particles, and additional supporting figures of SEM and STEM images have been included (PDF)

AUTHOR INFORMATION

Corresponding Author

*yi-lu@illinois.edu

ORCID

Yi Lu: 0000-0003-1221-6709

Notes

The authors declare no competing financial interest.

ACKNOWLEDGMENTS

The authors acknowledge Prof. Catherine J. Murphy, Prof. Kenneth S. Suslick, and Prof. Hong Yang for their insightful discussions. SEM, TEM, and STEM were carried out at the Federick Seitz Materials Research Laboratory Central Research Facilities, University of Illinois. The authors also thank Dr. Brian T. Sneed for suggestions in synthetic protocol, Vishwas Srivastava for help with HR-TEM and helpful discussions, Ryan J. Lake for proofreading the manuscript, and Kevin A. Harnden for his help with figure assembly.

REFERENCES

(1) (a) Qian, K.; Sweeny, B. C.; Johnston-Peck, A. C.; Niu, W.; Graham, J. O.; DuChene, J. S.; Qiu, J.; Wang, Y.-C.; Engelhard, M. H.; Su, D.; Stach, E. A.; Wei, W. D. *J. Am. Chem. Soc.* **2014**, *136* (28), 9842−9845. (b) Lewis, L. N. *Chem. Rev.* **1993**, *93* (8), 2693−2730. (c) Haruta, M. *Catal. Today* **1997**, *36*, 153−166.

(2) (a) Liu, J.; Lu, Y. *J. Am. Chem. Soc.* **2003**, *125* (22), 6642−6643. (b) Anker, J. N.; Hall, W. P.; Lyandres, O.; Shah, N. C.; Zhao, J.; Van Duyne, R. P. *Nat. Mater.* **2008**, *7* (6), 442−453.

(3) (a) Kauranen, M.; Zayats, A. V. *Nat. Photonics* **2012**, *6* (11), 737−748. (b) Wang, F.; Han, Y.; Lim, C. S.; Lu, Y.; Wang, J.; Xu, J.;

DOI: 10.1021/jacs.6b10983
J. Am. Chem. Soc. 2016, 138, 16542−16548

Chen, H.; Zhang, C.; Hong, M.; Liu, X. *Nature* **2010**, *463* (7284), 1061−1065.
(4) (a) Jain, P. K.; Huang, X.; El-Sayed, I. H.; El-Sayed, M. A. *Acc. Chem. Res.* **2008**, *41* (12), 1578−1586. (b) Hu, M.; Chen, J.; Li, Z.-Y.; Au, L.; Hartland, G. V.; Li, X.; Marquez, M.; Xia, Y. *Chem. Soc. Rev.* **2006**, *35* (11), 1084−1094. (c) Lal, S.; Clare, S. E.; Halas, N. J. *Acc. Chem. Res.* **2008**, *41* (12), 1842−1851. (d) Tao, Y.; Li, M.; Ren, J.; Qu, X. *Chem. Soc. Rev.* **2015**, *44* (23), 8636−8663. (e) Yu, M.; Zheng, J. *ACS Nano* **2015**, *9* (7), 6655−6674.
(5) Ortiz, N.; Skrabalak, S. E. *Langmuir* **2014**, *30* (23), 6649−6659.
(6) Chiu, C.-Y.; Ruan, L.; Huang, Y. *Chem. Soc. Rev.* **2013**, *42* (7), 2512−2527.
(7) (a) Seeman, N. C. *Nature* **2003**, *421* (6921), 427−431. (b) Alivisatos, A. P.; Johnsson, K. P.; Peng, X.; Wilson, T. E.; Loweth, C. J.; Bruchez, M. P.; Schultz, P. G. *Nature* **1996**, *382* (6592), 609−611. (c) Mirkin, C. A.; Letsinger, R. L.; Mucic, R. C.; Storhoff, J. J. *Nature* **1996**, *382* (6592), 607−609. (d) Jones, M. R.; Seeman, N. C.; Mirkin, C. A. *Science* **2015**, *347*, 1260901. (e) Tan, L. H.; Xing, H.; Lu, Y. *Acc. Chem. Res.* **2014**, *47* (6), 1881−1890. (f) Li, Y.; Liu, Z.; Yu, G.; Jiang, W.; Mao, C. *J. Am. Chem. Soc.* **2015**, *137* (13), 4320−4323. (g) Liu, Z.; Tian, C.; Yu, J.; Li, Y.; Jiang, W.; Mao, C. *J. Am. Chem. Soc.* **2015**, *137* (5), 1730−1733. (h) Zhang, F.; Nangreave, J.; Liu, Y.; Yan, H. *J. Am. Chem. Soc.* **2014**, *136* (32), 11198−11211.
(8) Sun, H.; Ren, J.; Qu, X. *Acc. Chem. Res.* **2016**, *49* (3), 461−470.
(9) (a) Wang, Z.; Tang, L.; Tan, L. H.; Li, J.; Lu, Y. *Angew. Chem., Int. Ed.* **2012**, *51* (36), 9078−9082. (b) Wang, Z.; Zhang, J.; Ekman, J. M.; Kenis, P. J. A.; Lu, Y. *Nano Lett.* **2010**, *10* (5), 1886−1891. (c) Song, T.; Tang, L.; Tan, L. H.; Wang, X.; Satyavolu, N. S. R.; Xing, H.; Wang, Z.; Li, J.; Liang, H.; Lu, Y. *Angew. Chem., Int. Ed.* **2015**, *54* (28), 8114−8118.
(10) (a) Wu, J.; Tan, L. H.; Hwang, K.; Xing, H.; Wu, P.; Li, W.; Lu, Y. *J. Am. Chem. Soc.* **2014**, *136* (43), 15195−15202. (b) Li, J.; Zhu, Z.; Liu, F.; Zhu, B.; Ma, Y.; Yan, J.; Lin, B.; Ke, G.; Liu, R.; Zhou, L.; Tu, S.; Yang, C. *Small* **2016**, *12* (39), 5449−5487.
(11) (a) Wang, D.; Li, Y. *Adv. Mater.* **2011**, *23* (9), 1044−1060. (b) Toshima, N.; Yonezawa, T. *New J. Chem.* **1998**, *22* (11), 1179−1201. (c) Liu, X.; Wang, D.; Li, Y. *Nano Today* **2012**, *7* (5), 448−466. (d) Gilroy, K. D.; Ruditskiy, A.; Peng, H.-C.; Qin, D.; Xia, Y. *Chem. Rev.* **2016**, *116* (18), 10414−10472.
(12) (a) Kimura-Suda, H.; Petrovykh, D. Y.; Tarlov, M. J.; Whitman, L. J. *J. Am. Chem. Soc.* **2003**, *125*, 9014. (b) Demers, L. M.; Östblom, M.; Zhang, H.; Jang, N. H.; Liedberg, B.; Mirkin, C. A. *J. Am. Chem. Soc.* **2002**, *124*, 11248. (c) Koo, K. M.; Sina, A. A. I.; Carrascosa, L. G.; Shiddiky, M. J. A.; Trau, M. *Anal. Methods* **2015**, *7* (17), 7042−7054.
(13) Chen, M.; Kumar, D.; Yi, C.-W.; Goodman, D. W. *Science* **2005**, *310* (5746), 291−293.
(14) Enache, D. I.; Edwards, J. K.; Landon, P.; Solsona-Espriu, B.; Carley, A. F.; Herzing, A. A.; Watanabe, M.; Kiely, C. J.; Knight, D. W.; Hutchings, G. J. *Science* **2006**, *311* (5759), 362−365.
(15) Lide, D. R. *CRC handbook of chemistry and physics: a ready-reference book of chemical and physical data*, 90th ed. (2009−2010. ed.); CRC Press: Boca Raton, FL, 2009.
(16) (a) Bower, M. M.; DeSantis, C. J.; Skrabalak, S. E. *J. Phys. Chem. C* **2014**, *118* (32), 18762−18770. (b) DeSantis, C. J.; Sue, A. C.; Bower, M. M.; Skrabalak, S. E. *ACS Nano* **2012**, *6* (3), 2617−2628. (c) DeSantis, C. J.; Peverly, A. A.; Peters, D. G.; Skrabalak, S. E. *Nano Lett.* **2011**, *11* (5), 2164−2168.
(17) (a) Weiner, R. G.; DeSantis, C. J.; Cardoso, M. B. T.; Skrabalak, S. E. *ACS Nano* **2014**, *8* (8), 8625−8635. (b) DeSantis, C. J.; Skrabalak, S. E. *J. Am. Chem. Soc.* **2013**, *135* (1), 10−13.
(18) (a) Laskar, M.; Skrabalak, S. E. *ACS Catal.* **2014**, *4* (4), 1120−1128. (b) Sneed, B. T.; Kuo, C.-H.; Brodsky, C. N.; Tsung, C.-K. *J. Am. Chem. Soc.* **2012**, *134* (44), 18417−18426.
(19) Habas, S. E.; Lee, H.; Radmilovic, V.; Somorjai, G. A.; Yang, P. *Nat. Mater.* **2007**, *6* (9), 692−697.
(20) Sabir, T. S.; Yan, D.; Milligan, J. R.; Aruni, A. W.; Nick, K. E.; Ramon, R. H.; Hughes, J. A.; Chen, Q.; Kurti, R. S.; Perry, C. C. *J. Phys. Chem. C* **2012**, *116* (7), 4431−4441.
(21) (a) Han, L.; Maye, M. M.; Leibowitz, F. L.; Ly, N. K.; Zhong, C.-J. *J. Mater. Chem.* **2001**, *11* (4), 1258−1264. (b) Njoki, P. N.; Luo, J.; Kamundi, M. M.; Lim, S.; Zhong, C.-J. *Langmuir* **2010**, *26* (16), 13622−13629. (c) Richards, V. N.; Rath, N. P.; Buhro, W. E. *Chem. Mater.* **2010**, *22* (11), 3556−3567.
(22) (a) Thanh, N. T. K.; Maclean, N.; Mahiddine, S. *Chem. Rev.* **2014**, *114* (15), 7610−7630. (b) Harada, M.; Kizaki, S. *Cryst. Growth Des.* **2016**, *16* (3), 1200−1212.
(23) Kennedy, T. A. C.; MacLean, J. L.; Liu, J. *Chem. Commun.* **2012**, *48* (54), 6845−6847.
(24) (a) Xia, Y.; Xia, X.; Peng, H.-C. *J. Am. Chem. Soc.* **2015**, *137* (25), 7947−7966. (b) Xia, X.; Xie, S.; Liu, M.; Peng, H.-C.; Lu, N.; Wang, J.; Kim, M. J.; Xia, Y. *Proc. Natl. Acad. Sci. U. S. A.* **2013**, *110* (17), 6669−6673.
(25) Straney, P. J.; Marbella, L. E.; Andolina, C. M.; Nuhfer, N. T.; Millstone, J. E. *J. Am. Chem. Soc.* **2014**, *136* (22), 7873−7876.
(26) Liu, J. *Phys. Chem. Chem. Phys.* **2012**, *14* (30), 10485−10496.
(27) Brown, K. R.; Natan, M. J. *Langmuir* **1998**, *14* (4), 726−728.
(28) Zhu, S.; Matilla, A.; Tercero, J. M.; Vijayaragavan, V.; Walmsley, J. A. *Inorg. Chim. Acta* **2004**, *357* (2), 411−420.

DOI: 10.1021/jacs.6b10983
J. Am. Chem. Soc. 2016, 138, 16542−16548